Transmissionless Selectively Aligned Surface-Permanent-Magnet BLDC Motor in Hybrid Electric Vehicles

Nirav P. Shah, Andrew Dorr Hirzel, *Member, IEEE*, and Baekhyun Cho

***Abstract*—An axial-flux permanent-magnet brushless motor is designed with variable stator alignment of independent stators, thus allowing field weakening via a controllable and variable generated-voltage constant. This feature is particularly valuable in vehicle traction motors with large constant-power speed ratio, where there is also a strong desire to eliminate the need for gear changes and keep the overall size of the motor drive as small as possible. The advantage of high pole count as applied to this technique is discussed, and the simulation impact on motor drive kilovoltampere, efficiency, gradability, acceleration, and maximum speed over typical driving cycles is shown.**

***Index Terms*—Brushless machines, field weakening, permanent-magnet (PM) motors, vehicle simulation.**

I. Introduction

AUTOMOTIVE vehicle performance is expensive and time consuming to fully test. It is often advantageous to simulate the results of vehicle performance with advanced modeling tools before committing to testing. This proposal undertakes vehicle level simulation to determine the value of the novel field weakening.

Vehicle performance is best described by a torque–power–speed curve similar to that shown in Fig. 1, which demonstrates that, at low driving speeds, a very high torque is required for acceleration and climbing steep grades and ramps. As travel speeds increase, less torque is required at which time the vehicle enters a constant-power region, which is the region where the vehicle traction power remains constant throughout the remaining speed range.

Gear ratio changes used in conventional drive trains allow the internal combustion engine to be used in the most advantageous torque versus speed region of engine performance. This advantage is immediately extended to electric motors. However, a desired solution is electric-driven drive trains without expense and efficiency-reducing gear ratio changes.

The constant-power region of Fig. 1 can be defined by the constant-power speed ratio (*CPSR*) [1]. *CPSR* is the ratio of the maximum vehicle speed divided by the speed at which the maximum torque is needed. Various traction applications require different *CPSR* values; for the purposes of this paper, a *CPSR* of four is pursued [2].

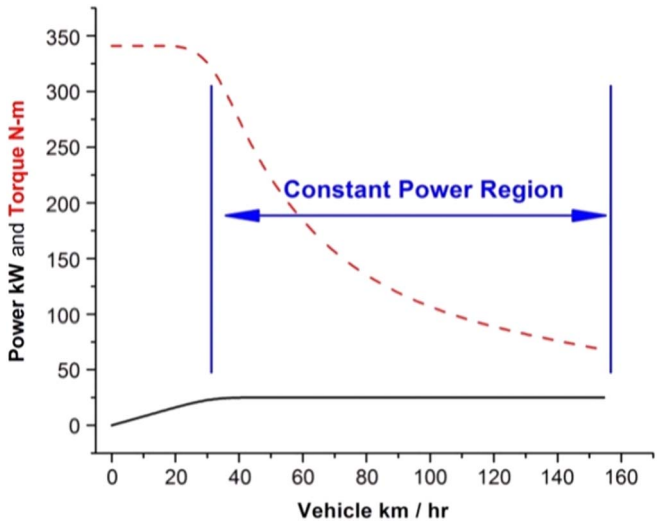

Fig. 1. Typical vehicle traction needs.

Although the *CPSR* of four is possible to obtain with induction and switched reluctance motor technologies, it is difficult, if not often impossible, to achieve with permanent-magnet (PM) technology without the use of gear ratio changes [3]–[5]. PM technology does, however, remain a superior choice for vehicle motors over induction and switched reluctance motor technologies because PM motors provide high power density and have inherent higher efficiency than other technologies [6].

An alternative to the gear ratio changes that can be used for all PM motors is to employ an oversized motor drive, measured in drive kilovoltampere. Applying this solution forces the oversized motor drive to provide very high currents necessary (at low voltages) for low-speed operation, which increase the cost and size of silicon switching devices (MOSFETs, insulated-gate bipolar transistors, etc.). However, at the highest speeds, the oversized motor drive must provide a very high voltage (and low current). This high voltage relates to the increase in costs of capacitance and other electronics. Ultimately, the motor drive cost is related to the product of the maximum current and maximum voltage needed throughout the entire operating range. Using an oversized motor drive together with an unweakened PM motor while attempting to address a high *CPSR* will result in a motor drive kilovoltampere to motor

Manuscript received February 28, 2009; revised October 22, 2009. First published November 13, 2009; current version published January 13, 2010.

N. P. Shah and B. Cho are with AVL Powertrain U.K. Ltd., SS15 6SR Basildon, U.K. (e-mail: nirav.shah@avl.com; harry.cho@avl.com).

A. D. Hirzel is with Light Engineering Inc., Indianapolis, IN 46268 USA (e-mail: ahirzel@Lt-Eng.com).

Color versions of one or more of the figures in this paper are available online at http://ieeexplore.ieee.org.

Digital Object Identifier 10.1109/TIE.2009.2036022

kilowatt ratio that is much larger than the *CPSR* value. In other per-unit terms, the motor of 1 kW will require a motor drive that is > 4 kVA. This solution is commercially unacceptable.

Another proposed alternative to gear ratio changes is to introduce into the motor a winding changeover technique. This technique is described in [7], where it is shown that a high degree of mechanical simplification can be achieved by the use of this technique. However, this technique has the additional cost of the necessary switches needed to reconfigure the coils, with a minimum of three switches per motor phase. In [8], it is shown that the number of switches can be reduced by the use of additional full-wave diode bridges. Both of these switching configurations can suffer from high-voltage transients in the dc link if care is not taken. Moreover, this technique allows only two discrete conditions and is not continuously variable.

Brushless PM motors can be divided into two broad categories: internal PM (IPM) and surface PM (SPM). The former is characterized by introducing magnetically soft material between the rotor's magnet pole and the air gap, whereas the latter has no such soft iron on the rotor. The soft magnetic material on the rotor of the IPM creates a condition where the Q- and D-axis inductances are substantially different. IPM motors have the ability to be effectively flux weakened through current-angle phase-advance techniques made possible by the large ratio between the Q- and D-axis inductances [9]. However, these flux-weakening techniques suffer from lower efficiency at flux-weakened high speeds and high frequencies.

With this phase-advance flux-weakening strategy, there is also a concern that the loss of current control while in this mode can result in extremely large instantaneous voltages from the uncontrolled electromotive force (*EMF*) [10]. Large instantaneous EMFs are generally permanently destructive to motor drive. Although IPM motors are popularly used with current-angle phase-advance techniques, rotor position detection errors can cause the high instantaneous EMF voltages and, thus, the destruction of the silicon devices of the motor drives. As used as a traction motor, this event can leave the vehicle operator stranded.

The typical SPM, on the other hand, is generally unsuitable to use with these current-angle phase-advance field-weakening techniques, having substantially identical Q- and D-axis inductances. Thus, this entire field of study cannot be employed on a class of high-efficiency and high-power-density motors.

Based on the aforementioned concerns, the goals of this paper are as follows.

1) To eliminate all gear ratio changes for the vehicle. This will increase the drive train efficiency and decrease the weight and cost of the vehicle. The use of a transmission in the vehicle will increase the overall vehicle weight. The transmission has losses associated with it, approximately 3%–8% loss [11] per gear mesh, depending on the number of gears and the gear selected, and thus, the overall efficiency of the drive train is also reduced.
2) To use an SPM as the traction motor application and intentionally avoid the use of current-angle phase-advance techniques. By avoiding this flux-weakened approach, the loss of control of rotor position will no longer be catastrophic to the operator and has the goal of assuring vehicle reliability.
3) To determine the smallest kilovoltampere to kilowatt ratio in the motor drive possible. This is done to reduce the overall vehicle costs.

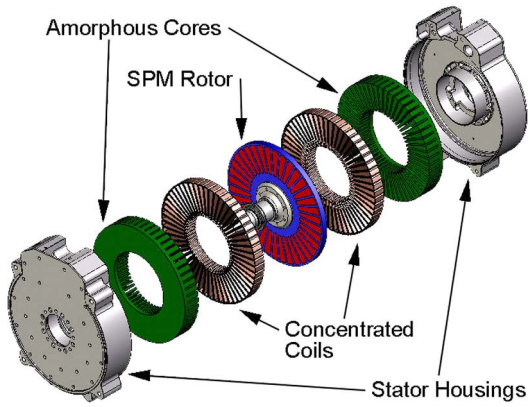

Fig. 2. AFIR-S topology.

Therefore, the goal of this paper is to eliminate all gear ratio changes in the vehicle using a brushless surface-mounted PM motor. For simplicity of the overall vehicle architecture and reduction in vehicle cost, a final drive ratio of 3.95 is initially selected for the single driving axle differential.

The difficulty in using a PM motor over wide speed ranges arises from the fact that the PM creates a permanent field. As speeds increase, the EMF generated increases in a linear manner. This is the fundamental reason why overly large motor drives are needed for high-speed motor operation.

Clearly, there is a desire to weaken the PM field as the motor speed increases. This weakening is easily accomplished in dc brush motors, as well as in induction motors. This is generally considered not feasible in SPM motors. This paper describes a novel and feasible means to provide SPM field weakening and describes the beneficial effects that this will have on vehicle cost.

II. Proposed Field Weakening

Field weakening for this paper will be accomplished by purely mechanical means of decreasing the overall *EMF* during higher speed operation. High speed is defined as any speed within the *CPSR* range, the CPSR being defined by the vehicle specification. This technique is referred as selectively aligned (SA).

The axial motor topology chosen has been described in [12] as an axial-flux internal-rotor external-stator PM slotted motor (AFIR-S), as shown in Fig. 2. This topology has the feature needed to implement the proposed SA field weakening, i.e., that there are two independent stators sharing a common rotor.

The stators are connected with like phases in series; therefore, the independently produced *EMF* waveforms from each stator will sum to create a phase *EMF* waveform that is effectively double in amplitude of either independent stator *EMFs*. In conventional use, the independent stators are typically fixed

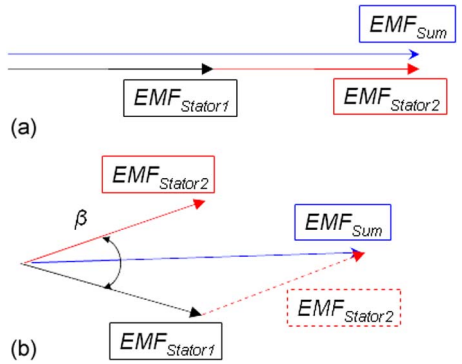

Fig. 3. Vectors describing change in *EMF*. (a) *EMF* completely aligned. (b) *EMF* weakened by β electrical degrees.

in position relative to one another. For SA field weakening, the stators will have their angular positions, measured in electrical degrees (β) and will be referenced to one another. It is thus possible to selectively choose β to purposely cause the like phases to be out of synchronization. This effect is shown in a vector diagram form in Fig. 3. The equations governing the mechanical degrees and the reduction in EMF are shown as related to β as follows, respectively:

$$EMF_{\text{Sum}} = (EMF_{\text{Stator 1}} + EMF_{\text{Stator 2}}) \cos\left[\frac{\beta}{2}\right] \tag{1}$$

$$\text{Degrees}_{\text{Mechanical}} = \frac{\beta}{\text{PolePairs}}. \tag{2}$$

This concept is discussed for the use with electronic control in [13]. An electronically controlled position actuator will be mounted to a fixed location of the stationary stator. The other end of the actuator will be mounted to the opposite stator. The opposite stator is free to rotate. With appropriate feedback to the electronic control (taken from the vehicle speed, for example), the actuator can be commanded to adjust the relative fixed-to-moving stator alignment over a given arc length. A small drive motor with a mating lead screw, as shown in Fig. 4, will provide adequate positional accuracy, as well as support the torque generated against the moving stator by the rotor during motoring operation.

The resulting electrical effect on the motor EMF of the selective alignment will be that of adding out-of-phase sine waves, resulting in a lower amplitude sine-wave EMF than that if completely in phase. The two stators each contribute EMF to the total EMF, and if aligned, the total EMF is added algebraically. However, when not directly aligned, the total is a vector sum. The alignment position "= zero position" produces the highest combined *EMFs* possible, while the opposite end of the alignment will be that of 180° (electrical) out of phase, which produces zero EMF.

It is for this waveform vector summing that, for optimum performance, pure-sine EMF is preferred from each stator. Since the sum of the independent sinusoidal waves results in a final sinusoidal wave with a distortion that will be, in some instances, amplified over and above the original distortion, pure sine is ideal and preferred.

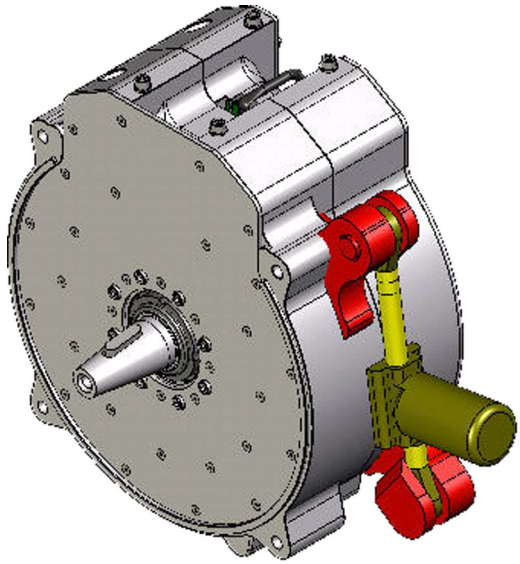

Fig. 4. Proposal shown with actuator.

Typically, the *EMF* is considered as a function of speed only, with the common term of Ke; this proposal will allow Ke to be a function of both speed and the amount of EMF reduction imposed by the selective alignment. Ke is an excellent widely used figure of merit to gauge motor performance.

An advantage of the SA field weakening is motor drive power electronics safety and vehicle reliability. The catastrophic failure mode described earlier for phase-advance flux-weakening techniques used for IPM motors is very unlikely using the proposed SA field-weakening technique, since the moving stator control will be on a discrete high-time-constant control device. With the proposed technique, in the event of loss of control of the actuator, the operator may experience one of the two worst case conditions. First, the operator may be required to "limp" with low speeds to a service station with a high-torque/low-speed motor (i.e., actuator locked at max Ke). The second mode of failure is the possibility of having a low-torque/high-speed motor (i.e., actuator locked at min Ke). In either event, the operator will certainly be able to avoid being stranded.

In addition to the need for the just-described independent stators, the AFIR-S topology is well suited in other aspects to implement the SA field-weakening method described in this paper. Other necessary aspects needed are as follows.

1) High-pole-count rotor. The high pole count results in a small mechanical angle for each PM pole pair. This reduces the arc distance that the actuator must travel to effect any given change in *EMF*. Shorter rotational distances are less costly to control, as well as more accurate. It is readily recognized that the AFIR-S is well suited for high pole count [14]–[16]. Moreover, the higher torque ripple sensitivity noted in [12] is greatly diminished by employing such a high pole count.
2) Low rotational losses. The motor will experience a high range of speeds and frequencies to fulfill the goal of the full *CPSR*. Since item 1) encourages the use of high pole count, the motor will naturally need to operate at high frequencies. Note that, although the output *EMF* may

TABLE I
BASELINE MOTOR PARAMETERS

Parameter	Value	Units
Line-Line Ke	0.67	Wb peak
Phase Resistance	0.0085	Ohm
Phase Inductance	0.036	milli-Henry
Pole Pairs	18	

be reduced via the SA field weakening, the stator cores will continue to experience full magnetic flux from the rotor and, therefore, full core losses resulting from PM rotor rotation. The motor solution must be designed for inherently low rotational core losses. AFIR-S designs can employ advanced low-core-loss materials [17].

3) Nearly ideal sine-wave output. The high pole count leads naturally to a near-sine *EMF* output. This is accomplished by employing a slot/phase/pole ratio of 0.5; EMF distortion can be designed to less than 5% [18].

III. DISCUSSION ON MOTOR PARAMETERS

A motor (model M32L2-005) built by LE Inc. was chosen for the study. This motor was selected for the obvious reason that it conforms to the main demand of the selective alignment concept: It is AFIR-S, as mentioned in Section II. This motor has 18 pole pairs, which is considered high pole count. The 18 pole pairs provide that the stator rotation required to completely negate the output EMF is just ten mechanical degrees. The motor is 32 cm in diameter; hence, if the full 10° rotation was required, it would require a stroke along a motor circumference of only 2.8 cm. This provides for very short actuation distance and allows fine and rapid control.

The M32L2-005 has a stator core material made from Metglas 2605SA1 ribbon that is manufactured and sold by Hitachi Metals. This is an amorphous iron ribbon that has extremely low core losses. The use of this material satisfies the requirement that the motor can tolerate a wide range of synchronous frequencies.

The final requirement that the motor has a slot/pole/phase ratio of 1/2 to provide low EMF distortion is also met.

The study will compare a baseline motor to an SA motor, with emphasis on suitability for vehicle application and an understanding of the efficiency of the applications over a typical operating range. The nonadjusted baseline motor used to make this comparison has the properties found in Table I.

The efficiency of the motor is critical to understanding the performance over the wide speed range. Failure to account for all of the losses will likely create a motor that can conceptually take advantage of the selective alignment but in practice is prone to destructive overheating at high speeds/frequencies. The proposed motor has been analyzed and tested for a variety of critical loss mechanisms.

Losses were calculated for the following:

1) rms copper winding losses;
2) skin and proximity effect losses in the copper windings from high frequency and carrier frequency;
3) core losses;
4) eddy current losses in PMs and rotor support structure;

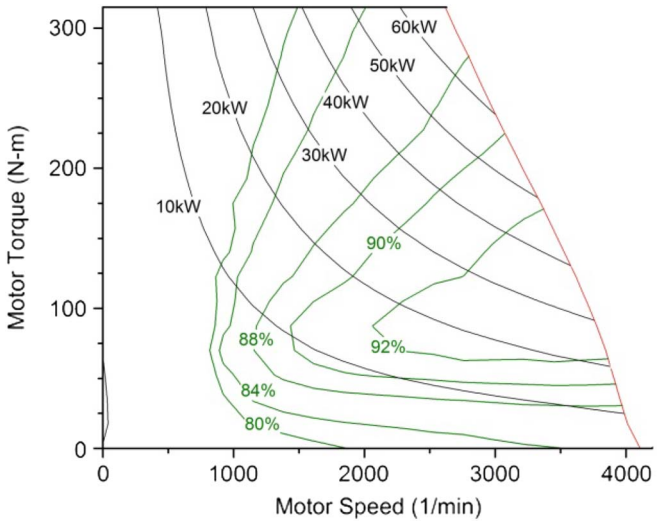

Fig. 5. Baseline motor performance.

TABLE II
SA MOTOR PROPERTIES

Parameter	Value	Units
Line-Line Ke (before any SA is applied)	0.92	Wb peak
Phase Resistance	.019	Ohm
Phase Inductance	.082	milli-Henry
Pole Pairs	18	

5) bearing losses;
6) windage losses.

The baseline motor was designed to reach the performance graph shown in Fig. 5. The steep decline in performance as high speeds are reached is a characteristic of any SPM motor, as the linear EMF approaches the fixed battery voltage, which, in this case, is 330-V dc.

The windings and Ke of the baseline motor were designed to reach the desired peak torque at base speed. With the goal of optimizing the use of SA, it is possible to propose the SA motor in Table II.

The parameters in Table II were achieved by a simple change to the parallel/series connections of the motor windings, much the same as standard 120 V/240 V changes are made in line-fed induction motors. In the same manner, it is therefore expected that there is no change to motor cost, mass, power, or efficiency from the winding changes from the baseline to SA motor. The change is only to the voltage/current relationship, to best take advantage of the SA concept. In each motor, there are 36 coils/teeth per phase. In the conventional motor, these are arranged as four teeth in series with nine parallel, whereas in the SA motor, these are six teeth in series with six parallel.

The SA motor was designed to reach the performance graph shown in Fig. 6. This performance required a maximum rotational selective alignment of 7.1 mechanical degrees necessary to keep the motor EMF below a 330-V dc battery limit. The degree of selective alignment was determined according to the relationship of the motor parameters, as well as the desired output power along with the CPSR, using the optimized method found in [19]. Notice that the shape of Fig. 6 closely resembles

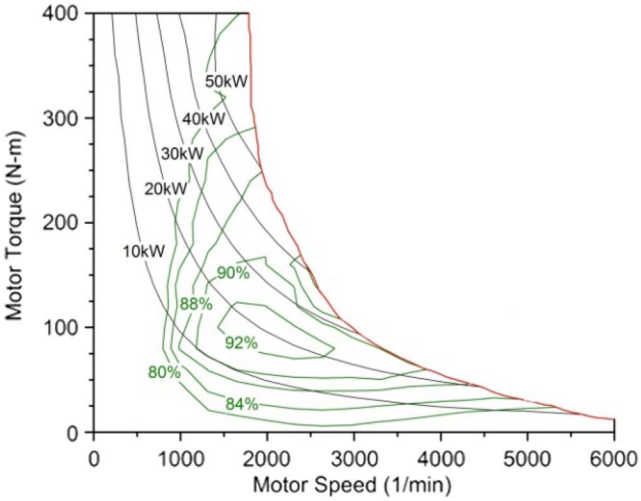

Fig. 6. SA motor performance.

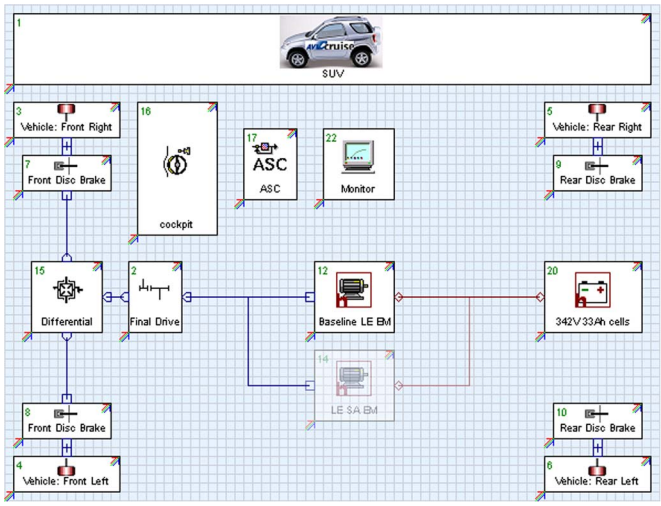

Fig. 7. EV model with both baseline and SA motors as shown in AVL Cruise software.

the desired performance shown in Fig. 1. This confirms that the SA concept has merit in better approximating end-use demands.

Both motors were modeled with identical weight, inertia, and cooling strategies.

IV. Simulation Setup to Determine Operating Range of Motors

Simulation results are obtained using AVL's vehicle systems and driveline analysis tool Cruise. AVL Cruise is used in drive train development to calculate and optimize fuel consumption, emissions, performance, transmission ratios, etc. The modular structure of Cruise permits modeling and simulation of all existing and future vehicle power train concepts, and a parametric evaluation of the various components can be performed.

The electric vehicle (EV) modeled in AVL Cruise is shown in Fig. 7. The complete vehicle model is combined from the Cruise built-in component model. Each component is then supplied with appropriate data. For example, the data required in the final drive model would be the gear ratio, inertia in and inertia out, efficiency, etc. In Cruise, the component models can be defined with varying fidelity. For example, the efficiency in the final drive model can be defined as fixed or varying with power input or output, or speed. The rigid mechanical connection between components is shown in blue lines, and electric connections are shown in red lines.

The bottom–left corner and top–right corner arrows are for component connections via a data bus. The typical data-bus use is to control the components by the information supplied by other components. For example, the electric motor model requires load signal/accelerator pedal signal from the cockpit model.

In the model shown, both the baseline and SA motors are shown for the sake of simplicity. While performing the simulation, only one electric motor at a time was virtually connected.

Closed-loop simulation model is considered in AVL Cruise. A drive cycle is input to the model, and a driver model (cockpit shown in Fig. 7) acts as the controller. It gives input to the brake and accelerator pedals for braking and to accelerate the vehicle, respectively, as demanded by the drive cycle. If the required demand from the drive cycle is met by all the power train components, then the vehicle follows the speed trace accurately. Battery and electric machine are the power train components modeled in details for an EV, apart from the detailed chassis, controller, etc., models. In this paper, our focus is on the electric machine; hence, we assume that battery will be able to provide the required power to motor at all times.

An electric machine model contains both the inverter and electric motor model.

The electric machine model is divided into three different sections.

1) Electrical: Losses like iron and copper and losses due to friction are calculated in this section.
2) Thermal: The complete power loss due to heat transition to the environment and heat power due to electric losses.
3) Mechanical: The mechanical torque output is calculated in this section. It takes acceleration demand as the input and losses from electrical and thermal sections of the model.

Inputs to the model are as follows:

1) inertia moment of the motor;
2) $drive + motor\ efficiency/power\ loss$ map;
3) torque–voltage map of the motor;
4) current–voltage map of the motor;
5) nominal voltage;
6) maximum current;
7) desired torque–controller input
8) ambient/external temperature–controller input.

Outputs from the model are as follows:

1) transient torque output to the driveline;
2) transient current required from the battery;
3) operating mode–generator/motor mode;
4) net voltage;
5) efficiency and/or power loss.

These outputs are used in the full vehicle model to run the closed-loop simulation and meet the speed trace as demanded by the drive cycle.

TABLE III
VEHICLE LEVEL MOTOR COMPARISON JUDGMENTS

Parameter	Value	Units
Maximum Grade		[%]
Maximum Grade [%]	@ 88kmph	[%]
Maximum Grade [%]	@ 72kmph	[%]
Maximum	Acceleration	[m/s2]
Acceleration time	0-80kmph	[sec.]
Maximum Speed	On level ground	[km/h]
Acceleration to	400 meters	[sec.]
Speed @	400 meters	[km/h]
Acceleration time to	1.6 km	[sec.]
Speed @	1.6 km	[km/h]
Average	Motor Eff.	[%]

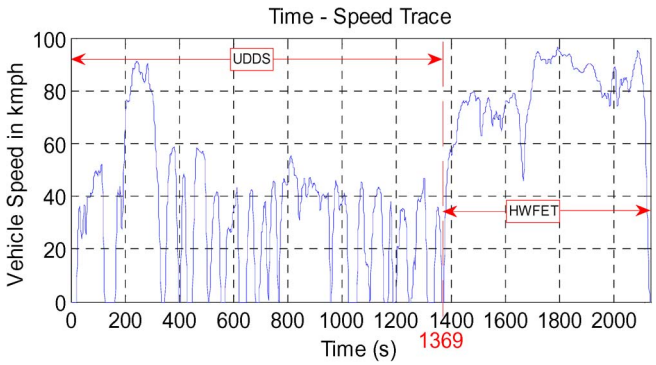

Fig. 8. Example of full drive cycle used; implementation of SAE J1634.

TABLE IV
EV AMERICA–U.S. DOE MINIMUM PERFORMANCE SPECIFICATIONS

Minimum Specification*	Speed	Values
Acceleration	0-80km/hr	13.5 sec
Minimum Top Speed	112 km/hr	0% grade
High Speed Gradability	88km/hr	3% grade
High Speed Gradability	72km/hr	6% grade
Minimum Gradability	1.5km/hr	25% grade
*These tests are done with curb weight of the vehicle plus 150kg		

The vehicle selection was a heavy SUV-type vehicle. The vehicle parameters are as follows:

1) SUV weight: 2000 kg;
2) $\mathrm{Cd} = 0.28$;
3) Frontal Area $= 2.25\ \mathrm{m}^2$;
4) Tire Rolling Radius $= 0.289$ m;
5) Final drive ratio $= 3.95$;
6) Driveline eff. $= 92\%$.

Table III describes the simulation outputs that the two motors will be judged against. These are metrics that are valid in that they are directly affected by electric motor selection.

In addition to the performance tests, the drive cycle defined in [20] was used for calculating the fuel economy and energy used by the EV. This is shown as time versus speed graph in Fig. 8. Both the UDDS and HWFET are parts of the EV America–U.S. Department of Energy (DOE) technical specification [21].

The minimum performance specifications for relevant tests are described in Table IV.

Shown in Fig. 9 is the distribution of motor torque–speed point matching the performance needed in Fig. 8. Note that, in

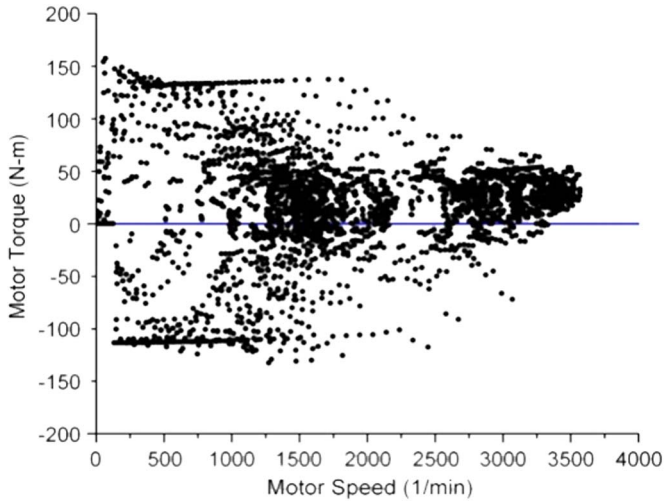

Fig. 9. Full drive cycle analyzed motor torque versus speed.

TABLE V
ANALYSIS RESULTS

Parameter	Baseline Motor	SA Motor	SA % improvement over Baseline
Max. Grade [%]	19.3	28.2	45.8
Max. Grade [%] @ 88km/hr	11.5	5.8	-50
Max. Grade [%] @ 72km/hr	13.9	7.9	-43
Max. Accln. [m/s2]	1.91	2.63	37.5
Accln. Time [s] (0-80km/hr)	14.3	14.1	1
Max. Speed [km/hr]	109.0	133.2	22
Accln. Time [s] to 400meters	23.0	22.3	3
Speed [km/hr] @ 400 meters	102.6	96.6	-6
Accln. Time [s] to 1600 meters	62.9	60.0	4.8
Speed [km/hr] @ 1600 meters	108.9	125.0	14.7

Fig. 9, each point represents 100 ms of vehicle operation. These points will be used to calculate motor efficiency.

V. RESULTS OF ANALYSIS

According to the vehicle parameters and tests defined in Section IV, the analysis results are presented. The vehicle was analyzed for various final drive ratios for both motor selections. Final drive ratios are typically chosen as a balance between maximum gradability and maximum speed. Final drive ratios from 2.5 to 4 were considered as typical for this type of vehicle.

Table V allows the comparison of the performance metrics proposed in Table III. The green cells in Table V show the improvement of the SA motor over the baseline motor. The cells in yellow show the improvement of the baseline motor over the SA motor.

It can be seen that the peak torque capability of baseline motor of approximately $100\ \mathrm{N \cdot m}$ less than the SA motor results in greater low-speed maximum gradability. For the vehicle specification discussed in Section IV, the maximum

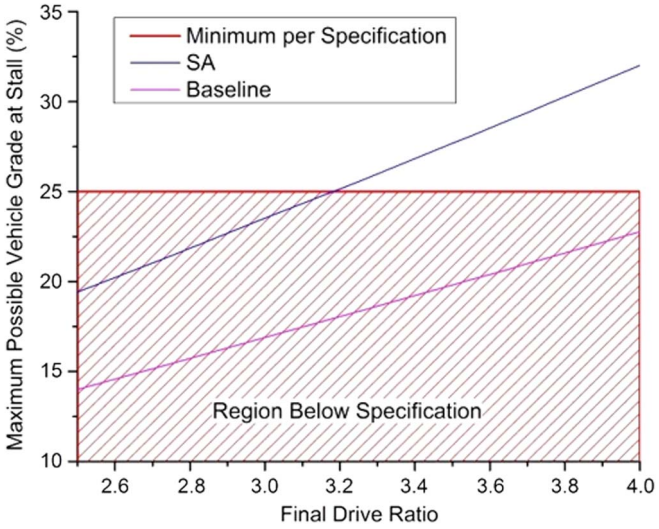

Fig. 10. Evaluation of final drive ratio versus maximum gradability requirement.

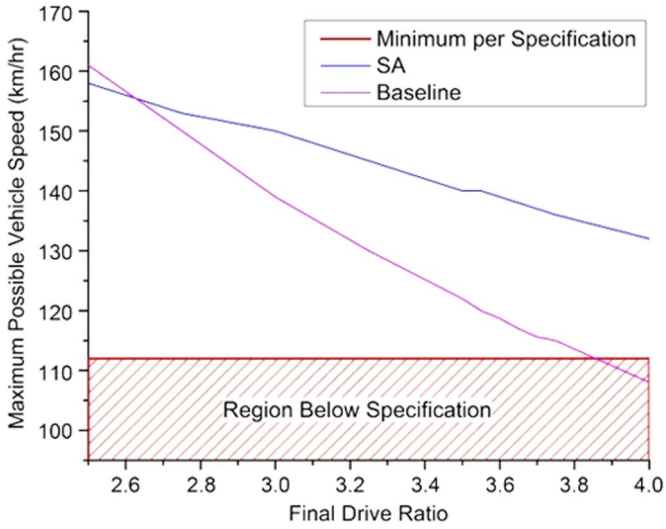

Fig. 11. Evaluation of final drive ratio versus maximum speed requirement.

gradability using the baseline motor is 19.31%, and using an SA motor, the gradability of vehicle increases to 26.94%. However, the gradability of the SA option does suffer at higher speeds of 72 and 88 km/h, although these are for speeds where the gradability is not generally needed.

The low-speed acceleration and maximum speed performance of the vehicle are improved to a considerable extent. As shown in Fig. 10, the 1999 EV-America performance specification for gradability of 25% can be achieved very easily using the SA motor.

Fig. 10 shows that the gradability requirement is not met with the baseline motor whatsoever. The SA motor meets the 25% gradability requirement for all ratios 3.25 and larger.

The second important requirement is the maximum speed. Fig. 11 shows that the maximum speed requirement of 112 km/h is met with the baseline motor for final drive ratios 3.75 and lower. The SA motor meets the 112 km/h requirement for all drive ratios considered.

TABLE VI
BATTERY AND MOTOR PERFORMANCE

Over 4 Drive Cycles	Baseline	SA	Improvement
Lumped Cycle Motor Efficiency	75.4%	76.3%	0.9%
Battery Depth of Discharge	40.7%	39.6%	1.2%

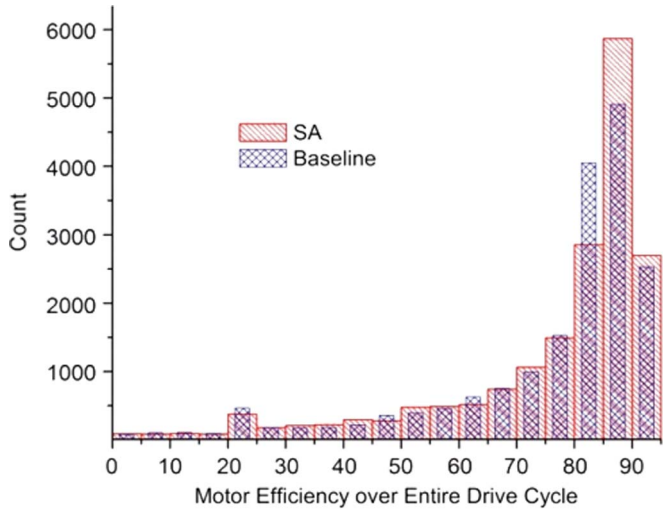

Fig. 12. Distribution of efficiency over drive cycle.

Thus, there is a clear tradeoff decision for the baseline motor. Either a high gradability (high acceleration performance) is achieved by a high final drive ratio or a high-speed range is achieved with a low final drive ratio. The latter is, however, at the expense of not meeting the minimum specification requirement.

On the other hand, for the SA motor, if greater performance (as in higher acceleration) is required, then a simple change to the selection of a higher final drive ratio will suffice. This can be done without sacrificing the maximum speed performance requirement of the standards specified in Table IV.

The SA motor meets both the maximum speed requirements of 112 km/h and minimum gradability of 25% for all drive ratios greater than 3.2. The baseline motor cannot meet the combined requirements with any drive ratio.

In Table VI, the overall lumped efficiency can be compared for the combined drive cycle run, when the final drive is kept with the same ratio of 3.95 and both the motors are run for the same drive cycle. The SA motor gives better overall system efficiency. This is shown graphically in Fig. 12. This clearly indicates that, for a specific distance, the vehicle with SA motor requires less battery size than the baseline motor or, that for the same battery size, the vehicle with SA motor can go a further distance than the vehicle with baseline motor. For the same distance, (four times the J1634 drive cycle; approximately 114 km), the battery final state of charge with the SA motor was 1.2% greater than with the baseline motor.

As can be seen from the baseline and SA motor plots in Figs. 5 and 6, respectively, the SA technology increases the maximum motor speed from 4000 to 6000 r/min. The increased maximum speed of the motor is important in light of the fact that there is a direct drive to the wheels. The increased motor speed relates directly to an increase in maximum vehicle speed

TABLE VII
DRIVE REQUIREMENT COMPARISON

Parameter	Baseline	SA	% Reduction
Battery Current			
Rated Operation	369	204	45%
Peak Operation	560	471	16%
Maximum Drive kVA at 330 VDC			
Rated Operation	122	67	45%
Peak Operation	185	155	16%

range if the available motor torque is sufficient enough at these high speeds.

The maximum motor speed in the vehicle equipped with baseline motor can be increased to 6000 r/min. This can be done by either having a smaller final drive ratio or by using two-geared transmission attached to the baseline motor. Either option will decrease the initial wheel torque capability, thereby reducing the already low gradability performance to unacceptable. For example, suggesting that the final drive ratio is decreased to 3 (from 3.95), although we will be able to meet the maximum speed performance, however, the low-speed gradability will decrease to 14%. Use of a two-speed gearbox was not considered; a two-speed gearbox is seen as having additional complexity, efficiency penalty, mass penalty, and cost increase.

It must also be noted that the goal of keeping the motor drive the same size or smaller in the comparison of the SA to the baseline motor was also achieved. To achieve rated conditions, Table VII demonstrates the important drive output parameters of battery current and overall drive kilovoltampere.

From Table VII it can be seen that the SA option will require a drive that is 1/2 the overall size of the Baseline operation. This fulfills a major goal of the study and will result in substantial cost savings for the vehicle.

VI. CONCLUSION

The introduction of SA motor, when compared to a baseline SPM motor, has been considered a complete success. The SA motor was superior to the baseline motor in the following simulated conditions.

1) The SA motor provided for a smaller kilovoltampere motor drive system than for the baseline motor. This is a primary benefit and exceeded the goal of merely maintaining the same size power electronics as the baseline system.
2) The SA solution did not require gear changes for a wide CPSR.
3) The SA solution also did not employ phase-advance flux weakening.
4) The SA motor was more efficient than the baseline motor over the simulation operating conditions, with a gain of 1/2% point. This exceeded the goal of merely maintaining the same efficiency as the baseline system.
5) The SA motor provided better simulated high-speed operation. This was a major goal of the study, to extend the high-speed range of the motor system without use of gear changes.
6) The SA motor provided better simulated gradability. This is the complement of the aforementioned goal, to extend the gradability/acceleration range of the vehicle without the use of gear changes.

The positional actuator system suggested to control SA is likely to be extremely robust and simple. There will be only two moving components, namely, the moving stator and the actuator rod of the positional device itself. The reliability and simplicity of these type control devices are similar, if not identical, to the actuators used for electric fly-by-wire aircraft wing flap systems. Hence, it is well proven that reliability and simplicity are achievable, the necessary engineering for that future study being to attain the appropriate reliability of an automotive application at the typical automotive cost point. The control electronics will be solid state and very simple, with one input and one output.

The simulated SA solution for traction motors in EV and hybrid EV (HEV) can be compared to the current complexity of automatic automotive transmissions, as the automatic transmission is a standard for continuously variable gear ratios for many traction applications. Although these transmissions are presently very robust, there are many moving parts, numbering in hundreds. It is expected that the SA solution will cost 1/4 as much as the conventional automatic transmissions. However, EV and HEV rarely adopt automatic transmissions and choose instead electronically controlled gear changing transmissions, as the former are inherently less efficient than the latter and also cause system difficulties for regenerative braking. However, the latter systems are even more complex than automatic transmissions. The SA solution proposed here is shown by simulations to provide smooth continuous changes to output torque similar to automatic transmission systems, but with less complexity, and also provide efficient regenerative braking as does an electronically controlled gear changing transmission, all while using a high-efficiency PM brushless motor.

REFERENCES

[1] S. W. Moore, K. M. Rahman, and M. Ehsani, "Effect on vehicle performance of extending the constant power region of electric drive motors," presented at the SAE Int. Congr. Expo., Detroit, MI, Mar. 1–4, 1999.
[2] J. Lawler, J. Bailey, J. McKeever, and J. Pinto, "Extending the constant power speed range of the brushless DC motor through dual-mode inverter control," *IEEE Trans. Power Electron.*, vol. 19, no. 3, pp. 783–793, May 2004.
[3] M. Ehsani, Y. Gao, S. Gay, and A. Emadi, *Modern Electric, Hybrid Electric, and Fuel Cell Vehicles: Fundamentals, Theory and Design*. New York: CRC Press, 2005.
[4] W. Cai, "Comparison and review of electric machines for integrated starter alternator applications," in *Conf. Rec. 39th IEEE IAS Annu. Meeting*, Oct. 3–7, 2004, pp. 386–393.
[5] K. Rahman and M. Ehsani, "Performance analysis of electric motor drives for electric and hybrid electric vehicle applications," in *Proc. Power Electron. Transp.*, Oct. 1996, pp. 49–56.
[6] J. F. Gieras and M. Wing, *Permanent Magnet Motor Technology*. New York: Marcel Dekker, 1997.
[7] C. H. Chen and M. Y. Cheng, "Implementation of a highly reliable hybrid electric scooter drive," *IEEE Trans. Ind. Electron.*, vol. 54, no. 5, pp. 2462–2473, Oct. 2007.
[8] T. Kume, M. Swamy, M. Sawamura, K. Yamada, and I. Murokito, "A quick transition electronic winding changeover technique," in *Proc. 35th*

Annu. IEEE Power Electron. Spec. Conf., Jun. 20–25, 2004, vol. 5, pp. 3384–3389.
[9] T. Jahns, "Flux-weakening regime operation of an interior permanent-magnet synchronous motor drive," *IEEE Trans. Ind. Appl.*, vol. IA-23, no. 4, pp. 681–689, Jul. 1987.
[10] N. Bianchi, S. Bolognani, and M. Zigliotto, "Analysis of PM synchronous motor drive failures during field weakening operation," in *Proc. 27th Annu. IEEE Power Electron. Spec. Conf.*, Jun. 23–27, 1996, vol. 2, pp. 1542–1548.
[11] M. A. Kluger and D. M. Long, "An overview of current automatic, manual and continuously variable transmission efficiencies and their projected future improvements," presented at the SAE Int. Congr. Expo., Detroit, MI, Mar. 1–4, 1999.
[12] M. Aydin, S. Huang, and T. A. Lipo, "Torque quality and comparison of internal and external rotor axial flux surface-magnet disc machines," *IEEE Trans. Ind. Electron.*, vol. 53, no. 3, pp. 822–830, Jun. 2006.
[13] A. D. Hirzel, "Selective alignment of stators in axial airgap electric devices comprising low-loss materials," U.S. Patent 7 034 427, Apr. 25, 2006.
[14] F. Profumo, Z. Zhang, and A. Tenconi, "Axial flux machines drives: A new viable solution for electric cars," *IEEE Trans. Ind. Electron.*, vol. 44, no. 1, pp. 39–45, Feb. 1997.
[15] N. Balkan Simsir and H. Bulent Ertan, "A comparison of torque capabilities of axial flux and radial flux type of brushless DC drives for wide speed range applications," in *Proc. IEEE Int. Conf. Power Electron. Drive Syst.*, 1999, vol. 2, pp. 719–724.
[16] A. Cavagnino, M. Lazzari, F. Profumo, and A. Tenconi, "A comparison between the axial flux and the radial flux structures for PM synchronous motors," in *Conf. Rec. 36th IEEE IAS Annu. Meeting*, Sep. 30–Oct. 4, 2001, vol. 3, pp. 1611–1618.
[17] A. Hirzel, "Synchronous design frequency as a free variable in permanent magnet brushless motors in effort to achieve optimal torque density," in *Proc. Int. Conf. Elect. Mach. Syst.*, Oct. 8–11, 2007, pp. 983–988.
[18] D. Hansleman, *Brushless Permanent Magnet Motor Design*., 2nd ed. Lebanon, OH: Magna Phys. Publishing, 2006.
[19] A. Hirzel, "Field weakened axial-gap surface permanent magnet traction motor design for constant power speed ratio," in *Proc. Int. Conf. Elect. Mach.*, Vilamoura, Portugal, Sep. 6–9, 2008, pp. 1–4.
[20] N. Shah and A. Hirzel, "Field weakened axial-gap surface permanent magnet motor for automobile traction use without gear ratio change," in *Proc. IEEE VPPC*, Harbin, China, Sep. 3–5, 2008, pp. 1–5.
[21] Surface Vehicle Recommended Practice—"Electric Vehicle Energy Consumption and Range Test Procedure," May 1993, SAE J1634 .

Nirav P. Shah received the B.E. degree in mechanical engineering from the University of Mumbai, Mumbai, India, in 2006 and the M.S.E. degree in automotive systems engineering from the University of Michigan, Dearborn, in 2008.

As an intern in 2007 and 2008 at LE Inc., Indianapolis, IN, he performed simulation and component specification of electric and hybrid electric vehicles. Since June 2008, he has been an Engineer with the Hybrid Systems Team, AVL Powertrain U.K. Ltd., Basildon, U.K., where he is currently involved in performing modeling, simulation, and analysis of various fuel saving concepts from engine stop–start systems to various hybrid power train architectures.

Andrew Dorr Hirzel received the B.S.I.O.E. degree from the University of Michigan, Ann Arbor.

He is the Chief Technical Officer with Light Engineering Inc., Indianapolis, IN, designing and optimizing high-frequency/high-power-density axial gap and amorphous metal motors for over nine years, resulting in 11 U.S. issued motor-related patents. The majority of his recent focus has been toward axial air gap brushless ac motors. Prior to his involvement with Light Engineering Inc., he worked in the rare-earth permanent-magnet industry in 1988.

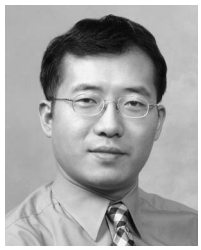

Baekhyun Cho received the B.Sc. and M.Sc. degrees from Seoul National University, Seoul, Korea, in 1989 and 1998, respectively.

In 1989, he was with Hyundai Motor Company for 15 years, where he worked on hydraulics, controls, and calibration of automatic transmissions and continuously variable transmissions. After his Ph.D. research at Cranfield University, Cranfield, U.K., he joined AVL Powertrain U.K. Ltd., Basildon, U.K., in 2006, where he is currently leading the Hybrid Systems Team in several engineering projects from major automotive original equipment manufacturers in the U.K. His research interests include power train modeling, fuel economy simulation, real-world usage analysis, and energy management of hybrid vehicles.